Myocardial Metabolism of Fluorodeoxyglucose Compared to Cell Membrane Integrity for the Potassium Analogue Rubidium-82 for Assessing Infarct Size in Man by PET

K. Lance Gould, Katsuya Yoshida, Mary Jane Hess, Mary Haynie, Nizar Mullani, and Richard W. Smalling

Department of Medicine, The University of Texas Medical School at Houston, Houston, Texas

Potassium loss from damaged myocardial cells is linearly related to CPK enzyme loss reflecting extent of necrosis. The potassium analog, rubidium-82 (^{82}Rb), is extracted after i.v. injection and retained in viable myocardium but is not trapped or washed out of necrotic regions. To compare myocardial cell metabolism with membrane dysfunction as indicators of necrosis/viability, 43 patients with evolving myocardial infarction and coronary arteriography had positron emission tomography using fluorodeoxyglucose (FDG) and the potassium analog ^{82}Rb. Percent of heart showing FDG defects and ^{82}Rb washout on sequential images indicating failure to retain the potassium analogue were visually assessed and quantified by automated software. Infarct size based on rubidium kinetics correlated closely with size and location on FDG images (visual r = 0.93, automated r = 0.82), suggesting that loss of cell membrane integrity for trapping the potassium analog ^{82}Rb parallels loss of intracellular glucose metabolism, both comparable quantitative markers of myocardial necrosis/viability.

J Nucl Med 1991; 32:1-9

Positron emission tomography (PET) identifies ischemic, viable, or necrotic/fibrotic myocardium by imaging rest-stress perfusion (*1*) or metabolic analogues, especially fluorine-18-fluorodeoxyglucose (FDG) depending on whether patients are fasted or glucose-loaded (*2–11*). Other markers of myocardial necrosis include release of myocardial CPK enzymes, inosine (*12,13*), phosphate (*14,15*), or potassium (*12–21*), but such approaches do not regionally locate and size the area of infarction or viability. The leak of potassium from myocardial cells is an immediate early marker of impaired cell membrane function and necrosis that has been well documented by a substantial literature (*12–21*). Therefore, a quantitative imaging method utilizing a potassium analogue reflecting cell membrane function might be useful for assessing viability and infarct size.

The intracellular-extracellular potassium gradient is maintained by intact myocardial cell membranes, the characteristics of which have been well documented (*16–23*). Damaged cell membranes associated with myocardial necrosis leak potassium from cells (*19–21*) into interstitial space (*17*) and venous effluent (*14–18*). The extent of potassium loss from myocardial cells is directly and linearly related with CPK enzyme loss (*18, 20,21*), reflecting extent of necrosis. In addition to being a marker of necrosis, radioactive potassium, ^{43}K, has been well studied for myocardial imaging (*23–26*).

Rubidium is a potassium analog with a variety of medically useful radioactive forms including ^{81}Rb, ^{82}Rb, ^{84}Rb, and ^{86}Rb. Myocardial cell membrane transport, trapping, and flow-extraction characteristics of potassium and rubidium parallel each other (*27–34*). Rubidium tracers have also been used for measuring perfusion in animals (*29–46*) and in man (*47–54*). For PET imaging, the strontium-82/rubidium-82 generator has been developed (*55*) and adapted for commercial production (*56*). Clinically, it is useful for qualitative infarct imaging (*54*) and has high sensitivity/specificity for diagnosis of coronary artery stenosis and its severity (*57,58*). Therefore, the behavior and kinetics of rubidium in myocardium are well established.

The basis for using ^{82}Rb in assessing viability and infarct size has also been demonstrated in animals (*59*). Upon delivery by coronary flow to myocardium, rubidium enters normal cells where it is trapped. However, if these cells are necrotic (TTC negative), the delivered rubidium leaks or washes out of the cells. In dogs with myocardial infarction and reperfusion, myocardial ru-

Received Jan. 22, 1990; revision accepted Jul. 19, 1990.

For reprints contact: K. Lance Gould, MD, Division of Cardiology, Room 4.258 MSMB, University of Texas Medical School at Houston, Houston, Texas 77225.

bidium washout measured by beta probes over the 120–240-sec after i.v. injection identifies necrotic versus viable myocardium with high reliability and little overlap (*59*).

Based on these prior reports, the current study was carried out to determine in patients with myocardial infarction (MI) whether cell membrane dysfunction as evidenced by abnormal kinetics of the potassium analogue ^{82}Rb parallels abnormal intracellular metabolism of the glucose analogue, FDG. This question is important for an integrated understanding of how we identify viable versus necrotic myocardium in clinically applicable physiologic terms. An important associated question on the quantitative relation of metabolic and membrane function was: Does the size of myocardial infarct showing a rubidium leak measured in man by PET equal the size of MI showing abnormal glucose metabolism measured by FDG imaging?

METHODS

Patient Population

Study subjects were 43 male or female patients hospitalized for suspected MI ruled in or out by characteristic ECG and/or CPK enzyme changes. Coronary arteriography was obtained in all patients for clinical reasons by the percutaneous transfemoral route. Patient selection depended primarily on availability of an ^{82}Rb generator, availability of FDG, consent of patient and attending physician, availability of attending and technical staff, and adequate scanner function. A mix of patients with recent or old MI were selected in order to make the study population comparable to that seen in clinical practice. The median time between MI and the PET scan was 27 days with a range of 4 days to 72 mo. Twenty-two patients had MI within 1 mo prior to the PET scan and 21 patients more than 1 mo prior to PET studies. Therefore, the study population included a balanced range of infarct ages characteristic of a clinical practice. PET studies were carried out after informed consent, approved by the University of Texas Committee for the Protection of Human Subjects, was obtained.

Rubidium-82 Kinetics for Assessing Myocardial Necrosis/Viability

The clinical protocol based on rubidium kinetics is illustrated in Figure 1. It divides resting PET data collected in list mode into an early image (first 15–110 sec) and a late image (all data after 120 sec). A new defect or worsening defect on the late image compared to the early image indicates washout or failure to trap rubidium and therefore necrosis. Residual myocardial trapping of rubidium on the late image within a defect reflecting partial or limited washout indicates some residual viable myocardium.

The basis for automated quantitation of infarct size by PET based on kinetics of ^{82}Rb is shown in Figure 2. Viable myocardium traps rubidium with no washout from a region of interest on the time-activity curve (upper panel). Infarcted myocardium fails to retain rubidium, which washes out from cells after initial uptake (middle panel). A mix of infarcted and viable tissue in the field of view results in an intermediate

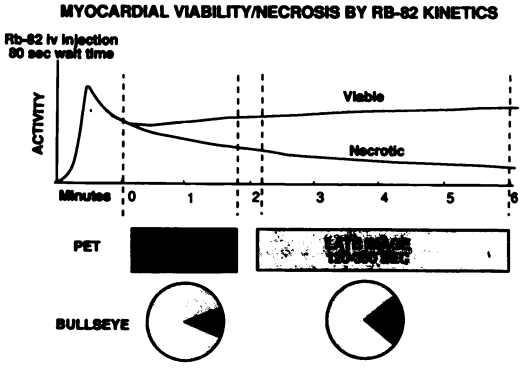

FIGURE 1
Schematic of the clinical protocol utilizing the kinetic changes of ^{82}Rb after i.v. injection for assessing myocardial viability.

level of washout proportional to the percent of viable or infarcted tissue. The activity in the late (S2) rubidium image relative to the early (S1) image reflects the extent of washout and proportion of viable or necrotic myocardium.

In order to avoid questionable assumptions of complex models, we used a simple measurement scheme to quantify rubidium washout where percent viable myocardium is equal to the ratio of activity in the late to the early image, corrected for background activity, written as $\%V = (S2\text{-}B)/(S1\text{-}B)$. By rearranging this simple expression, an equation is obtained (Fig. 2), relating the late/early activity ratio (S2/S1) to percent viability, $S2/S1 = \%V + [B\text{-}B\ (\%V)]/S1$. Since it cannot resolve left ventricular subendocardial-subepicardial differences, PET imaging shows mean transmural radionuclide distribution. Defining MI on the basis of decreased transmural radionuclide uptake therefore requires choosing some arbitrary degree of necrosis through the left ventricular wall that is defined as "infarction." Therefore, for purposes of objective automated infarct sizing, we then defined necrotic myocardium as less than 50% viable tissue in any given segment of myocardium. Accordingly, the value of V in the above equation was chosen to be 50%.

Due to the combination of spillover, partial volume errors, positron range, and background activity, an average of 55% of maximum activity remains in the most severe perfusion defects (scar) on PET scans of rubidium and/or FDG. Accordingly, the value of B in the above equation was chosen to be 55%. Average activity of normal myocardium is typically 85% of maximum activity on rubidium PET scans under resting conditions. Substituting these values into the equation of Figure 2 gives the relative S2/S1 threshold, 0.825, below which myocardium was defined as necrotic. Percent of the myocardium that was infarcted as defined above was then automatically determined from the polar map display of the relative S2/S1 ratio image as that percent of the relative S2/S1 polar map falling below the threshold of 0.825. For scarred myocardium with occluded coronary arteries, the initial delivery of tracer may be negligible on early and late images, thereby causing a defect comparable to background. Since activity in such severe defects is so low in the early image, there is no further washout due to activity at background levels. For such cases (2 of 43 patients), size of MI was defined as percent of myocardium with less than 55% of maximum activity, just as for FDG images.

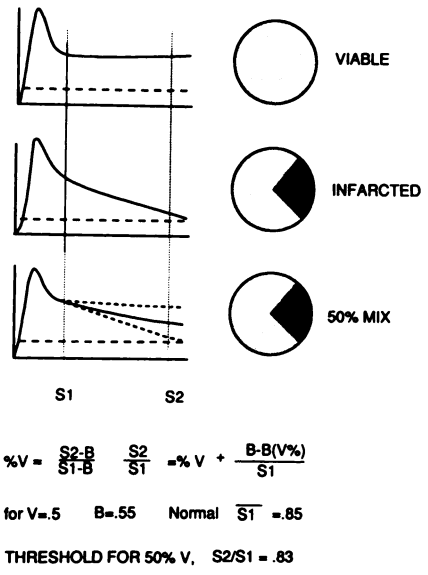

FIGURE 2
Basis for automated quantitation of infarct size by PET based on the kinetics of ^{82}Rb.

Our ratio of late-to-early myocardial activity (S2/S1) is a measure of myocardial washout because (a) images are obtained temporally later (95–190 sec after injection) than blood-pool activity for arterial input (0–40 sec) and (b) the regional myocardial ratio S2/S1 is used, *not* myocardial-to-blood pool ratio as calculated for perfusion.

FDG for Assessing Myocardial Necrosis/Viability

In the literature, cardiac FDG imaging has been carried out after both fasting and oral glucose loading. Because the literature is unclear as to the merits of fasting or glucose loading by direct comparison in the same subject, six patients had two sequential resting cardiac FDG images on separate days obtained after fasting and oral glucose loading. As described in the Results, FDG imaging at rest under fasting conditions is often uninterpretable. Consequently, in our laboratory, for the clinical question of whether myocardium is viable versus necrotic/scar, we obtain PET images of myocardial FDG after an oral *glucose load* when both normal and ischemic myocardium take up FDG but necrotic tissue does not (*2–4*); the glucose-loaded protocol does not separate ischemic from non-ischemic normal myocardium. For the question of whether myocardium is ischemic, we obtain PET images of FDG injected intravenously after *fasting* and during exercise (or at rest for this study) when ischemic viable myocardium traps FDG but necrotic and normal myocardium do not (*2,5–10*); the fasting protocol does not separate normal nonischemic from necrotic myocardium. Either one or both of these protocols are used for clinical purposes to decide on interventions after MI either with or without reperfusion (glucose-loaded, viability protocol) or for assessing stenoses of equivocal severity (fasting, exercise ischemia protocol).

Since under glucose-loaded conditions, ischemic viable and normal nonischemic myocardium both take up FDG, perfusion imaging at rest is carried out first to identify underperfused areas. Viable areas are then defined by a flow-metabolism mismatch (perfusion defect, normal FDG uptake) and non-viable areas as a flow-metabolism match (perfusion defect, FDG defect) (*2*).

Patients with underperfused, viable myocardium identified by FDG uptake demonstrated improved left ventricular function after bypass surgery (*3*). For patients having recent MI, 75%–80% of patients and 50%–68% of myocardial segments have significant remaining viable myocardium (*3,4,9,11*), 85% of which demonstrate improved contractile function after reperfusion (*3*).

PET Imaging Protocol

For the viability-infarct size protocol, non-fasted patients were given 50 g of oral glucola on arrival in the PET laboratory. Diabetic patients had their usual breakfast and insulin or oral hyperglycemic drugs in their usual doses. Twelve standard ECG leads and Dynamap blood pressure cuffs were attached for monitoring each patient throughout the study. Heart borders were marked by fluoroscopy and the patient was positioned in the PET scanner. Using a ring of gallium-68, a transmission scan was obtained over 25–30 min containing 200 million counts. Forty to 50 mCi of ^{82}Rb was infused intravenously from a strontium-82/rubidium-82 generator (Squibb, Princeton, NJ) over 30–60 sec. The generator was eluted daily for calibration and for strontium breakthrough, which did not occur.

Data collection of rubidium activity was begun in list mode at 80 sec (defined as zero time of data collection) after the beginning of ^{82}Rb infusion to allow for blood-pool clearance and continued through 360 sec. The first 15 sec of data were discarded and the early phase image was collected 95–190 sec after injection or 15–110 sec after beginning of data collection. Early and late images were reconstructed using the first 15–110 sec and 120–360 sec of data collection, respectively. During the fixed 6-min data collection, typically 15–25 million counts were obtained. Each original nine-slice image set of early and late data were reformatted into true short-axis, true long-axis, and polar maps in paired side-by-side displays as previously reported (*60*). A relative ratio image of the late-to-early polar maps was also displayed as a ratio polar map (relative S2/S1) for quantitative analysis.

After completion of rubidium imaging, 10 mCi of [^{18}F] FDG was injected intravenously. Forty-five minutes later, data collection of the FDG images was started, lasting 30 min with acquisition of approximately 30 million counts per whole-heart data set.

For the myocardial ischemia protocol, patients were fasted for 16 hr before the study and no glucola was given, the remainder of the protocol being the same as for the glucose-loaded viability protocol. FDG images were processed into true short- and long-axis views and polar map displays in a paired side-by-side comparison to the late rubidium images.

Data Acquisition

PET images were obtained on the University of Texas nine-slice, prototype, positron emission tomograph as described previously (*57–64*) and used in over 1250 patient studies on clinical protocols. This tomograph utilizes cesium fluoride detectors and a narrow coincidence window of 6 nsec that reduces randoms and increases count rate capacity essential for obtaining adequate image counts with ultrashort half-life tracers. Reconstructed resolution was 14 mm consistent with the range of heart motion on ungated images. Second- and

third-order cross coincidences were used to improve axial sampling. Resolution and sensitivity were uniform to within ±10% throughout the field of interest.

Data Analysis

Polar map displays were normalized to the mean top 2% of activity in each whole-heart polar map display as previously described (*60*). The size of the infarcted area was automatically determined as percent of the rubidium S2/S1 ratio image that was less than 0.825, as described above.

Since many of our patients had undergone reperfusion therapy for acute MI, the concept of a perfusion-metabolism mismatch (perfusion defect, FDG uptake) to define viable myocardium or a perfusion-metabolism match (perfusion defect, FDG defect) to define necrotic myocardium was not clearly applicable. Accordingly, the size of the infarcted area on the FDG image was automatically determined as the percent of the FDG polar map display that was less than 55% of maximum FDG uptake in that polar map.

Images were also visually interpreted independently by two experienced PET observers blinded to clinical and arteriographic data. Visual estimates of infarct size as percent of the left ventricle were also made from the tomograms and polar map display of paired late/early rubidium images and paired late rubidium/FDG images. Correlations between infarct size by visual estimates and by the automated technique for late/early rubidium and FDG images were made using linear regression (*65*).

RESULTS

Forty-three patients were studied, 36 with rubidium and FDG after glucose loading. Seven of the 43 were studied with FDG after glucose loading and again with FDG after fasting in order to compare the merits of the glucose-loaded viability protocol with the fasting ischemia protocol in the setting of acute evolving MI.

Figure 3 shows early (S1) and late (S2) images after a single i.v. injection of generator-produced ^{82}Rb in a patient with an evolving acute inferior myocardial infarction in true short-axis views (Fig. 3A), and in horizontal and vertical long-axis views (Fig. 3B). The number after the decimal is the image plane for both studies 1 and 2. In the color coding, white indicates the highest activity, red next highest, yellow intermediate, with green and blue as the lowest relative activity. In true short-axis views in Figure 3A, the image planes are arranged from the AV ring at the upper left to the apex at the lower right. The anterior wall is at the top of each image, the free LV wall is on the left, and the septum is on the right of each tomograph.

Tomographic data are summarized in a polar display (Fig. 3B). Polar displays on the left (lower half of figure) show the relative activity on a scale of 0%–100% with the early study as the upper (S1) and the late study as the lower (S2) of the polar maps on the left side of the panel. The lower right polar display, labeled relative S2/S1 ratio, shows the relative change in normalized activity of the late image divided by the relative distribution of normalized activity of the early image (relative instead of absolute values), on a scale of 0–2. It therefore quantifies the relative change in activity from early to late images. The upper right polar map labeled absolute S2/S1 ratio is used for comparing rest-stress images and has no meaning or use for comparing early-late images.

In Figure 3B the early rubidium image (S1) shows some perfusion to the inferior wall that washes out to leave a severe defect indicating necrosis in this area. Letters and numbers beside each polar map show quantitative results. The numbers beside the rubidium relative S2/S1 polar display of Figure 3B (lower right) indicate the % of the polar map (W = whole LV) below the 0.825 threshold, shown on the lower right polar map as 10% of the left ventricle. The inferior infarct on the FDG image (S2) of Figure 3C is the same as on the late rubidium image (S1). Infarct size by FDG shown beside the lower left (S2) polar map indicates that 13% of the heart failed to take up glucose and was therefore necrotic, also inferiorly.

Figure 4A correlates the visually estimated infarct size on rubidium and FDG images. However, to avoid possible observer bias, the automated infarct sizes by rubidium and FDG were also correlated as shown in Figure 4B. The patients with very large infarct areas had previous infarctions and severe ischemic cardiomyopathy and were under consideration for cardiac transplantation. For these large infarct areas, the relation between infarct size by rubidium and FDG is less good. Either the ^{82}Rb method underestimates the very large infarcts or the FDG method overestimates their size. Since the largest infarct sizes of 80% by FDG (but smaller by ^{82}Rb washout) would generally be considered incompatible with survival, the 80% infarct size by FDG may be an overestimate due to lack of myocardial uptake in some viable areas as occurs in up to 20%–25% of hearts for reasons other than MI.

In one patient, with the smallest infarct by FDG, the late rubidium and FDG images appeared visually identical but the FDG activity in the infarct areas was just above the 55% threshold for automated determination of size; therefore, the automated infarct size by FDG was smaller than the visual size of the infarct on both FDG and rubidium images.

Of the 36 patients with FDG and rubidium studies, there were six patients in whom there was no or little uptake of FDG by myocardium, the activity being entirely or primarily in blood pool in four patients. In the remaining two of these six patients, part of the normal myocardium took up FDG but large areas of the left ventricle failed to take up FDG despite normal contractile function on left ventricular angiogram and normal resting flow (no perfusion defect) through non-infarct related, normal, or minimally narrowed coronary arteries. All six of these patients were diabetic treated with either insulin, oral hypoglycemic agents,

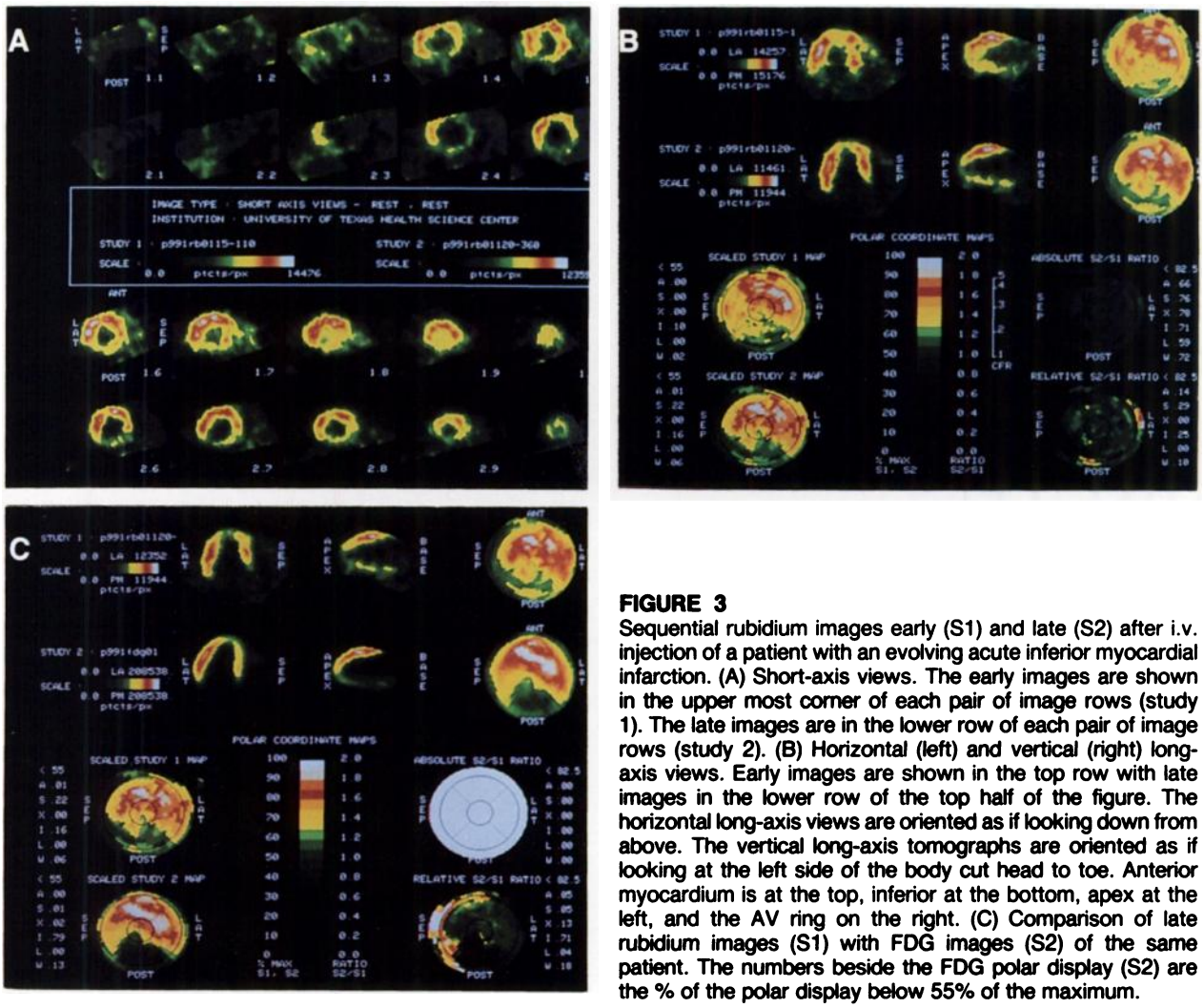

FIGURE 3
Sequential rubidium images early (S1) and late (S2) after i.v. injection of a patient with an evolving acute inferior myocardial infarction. (A) Short-axis views. The early images are shown in the upper most corner of each pair of image rows (study 1). The late images are in the lower row of each pair of image rows (study 2). (B) Horizontal (left) and vertical (right) long-axis views. Early images are shown in the top row with late images in the lower row of the top half of the figure. The horizontal long-axis views are oriented as if looking down from above. The vertical long-axis tomographs are oriented as if looking at the left side of the body cut head to toe. Anterior myocardium is at the top, inferior at the bottom, apex at the left, and the AV ring on the right. (C) Comparison of late rubidium images (S1) with FDG images (S2) of the same patient. The numbers beside the FDG polar display (S2) are the % of the polar display below 55% of the maximum.

or dietary regimens. Since these six FDG images were uninterpretable, they were excluded from the quantitative analysis comparing FDG to rubidium.

In three additional patients, FDG and rubidium images were markedly discordant due to defect size on FDG images that were grossly larger visually and by automated sizing than on rubidium images; this large defect size on FDG images was caused by lack of FDG uptake in myocardial areas of normal left ventricular contraction and normal perfusion by noninfarct-related, normal, or mildly narrowed coronary arteries. Two of these three patients were also diabetic. However, these three patients with aberrant absence of regional FDG uptake were included in the quantitative comparison of the FDG with rubidium for infarct sizing since at least substantial parts of the myocardium took up glucose appropriately.

There was visual concurrence in location, essential interpretation, and visual size of the infarct area on rubidium and FDG images in 27 of the 27 remaining patients in whom FDG was normally taken up by normal areas of myocardium not involved in the infarction. In 2 of these 27 patients, the essential visual interpretation was the same but the infarct size on the FDG image was somewhat larger than by rubidium, both of whom had no FDG uptake in small areas of normal left ventricular contraction and perfusion by noninfarct-related arteries. Conservatively, for the quantitative comparison of infarct size on rubidium with FDG images, only the six patients with unusable FDG images were excluded, leaving 30 of the 36 patients with paired FDG and rubidium studies, including those with some regional deficiency of FDG uptake despite normal contraction and perfusion through noninfarction-related arteries to those areas. The agreement between infarct size by FDG and ^{82}Rb was independent of infarct age and held true over the full range of times between infarction and PET scans.

Thus, out of 43 patients with acute-evolving MI studied with FDG after glucose loading, 9, or 21%, had no myocardial uptake anywhere in the heart or large areas of normal myocardium that did not take up

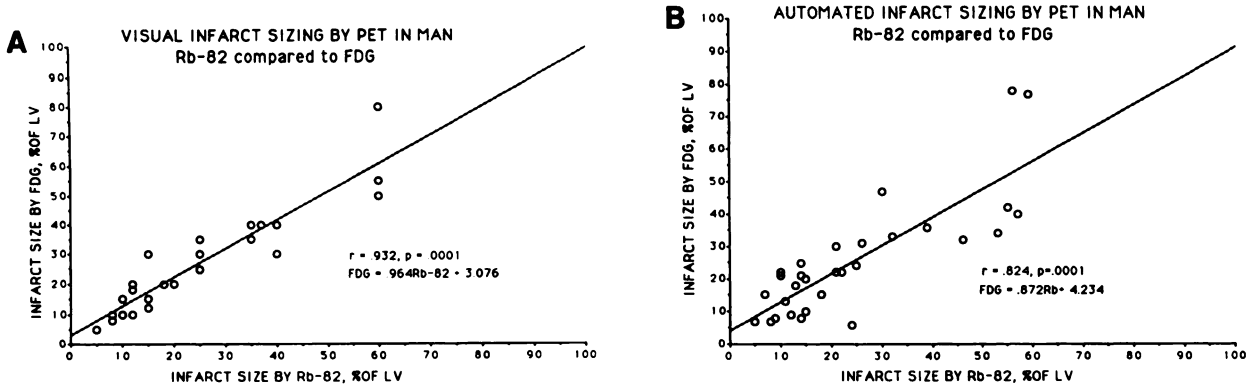

FIGURE 4
(A) Relation of visually estimated infarct size by rubidium and FDG imaging. (B) Relation of infarct size by the automated threshold method using rubidium and FDG images.

glucose after glucose loading despite normal contraction and perfusion. Eight out of these nine were diabetic.

Of the seven patients studied with FDG after a 16-hr fast, two failed to take up FDG anywhere in the heart either after fasting or glucose loading; five showed intense FDG uptake in areas of infarcted myocardium, as defined by (a) a severe defect or lack of FDG uptake on glucose-loaded images in contrast to normal myocardium which did take up FDG, (b) akinesis on left ventricular angiogram in the area of the defect on perfusion and glucose-loaded FDG images, and (c) arterial occlusion, severe stenosis, and/or intraluminal clot in the infarct-related artery by arteriography. Figure 5 illustrates the phenomenon of intense FDG uptake by recently infarcted myocardium. The upper of each pair of tomographic rows (S1) shows FDG images after glucose loading. The lower row of each pair (S2) shows FDG images after fasting. Under glucose-loaded conditions, the normal myocardium took up FDG but the infarct area failed to take up FDG, corresponding to an akinetic anterior wall and an occluded LAD at arteriography. After glucose loading, the normal myocardium took up FDG with peak activity of 103,973 cts/pixel.

However, after fasting this same area of necrosis took up FDG intensely, with a peak activity of 101,913 cts/pixel. Therefore, the intensity of FDG uptake in the necrotic area after fasting is not due to relative upscaling of image intensity referenced to suppressed FDG uptake in normal myocardium. Rather, it is due to intense FDG uptake in an area of infarcted myocardium which is so intense that it downscales relative intensity of the rest of the image.

DISCUSSION

These results suggest that in myocardial necrosis in man the loss of cell membrane integrity as reflected by abnormal kinetics of the potassium analog, ^{82}Rb, parallels loss of intracellular intermediary glucose metabolism as reflected by a lack of FDG uptake. In addition, the size of infarcted myocardium defined by abnormal rubidium kinetics is comparable to the size of infarcted myocardium defined by a lack of FDG uptake on PET images. Our observations extend the well described behavior of potassium as a marker of myocardial necrosis into clinical application for infarct sizing and relates it to more recent measures of viability based on metabolic imaging. Thus, myocardial necrosis or viability may be identified by measures of either glucose metabolism or cell membrane integrity.

Limitations of the Methodology

We observed several circumstances where myocardial FDG uptake may not be consistent and is therefore difficult to interpret for differentiating necrotic from viable tissue. Normal myocardium of *diabetic patients* may not take up FDG either with or without glucose

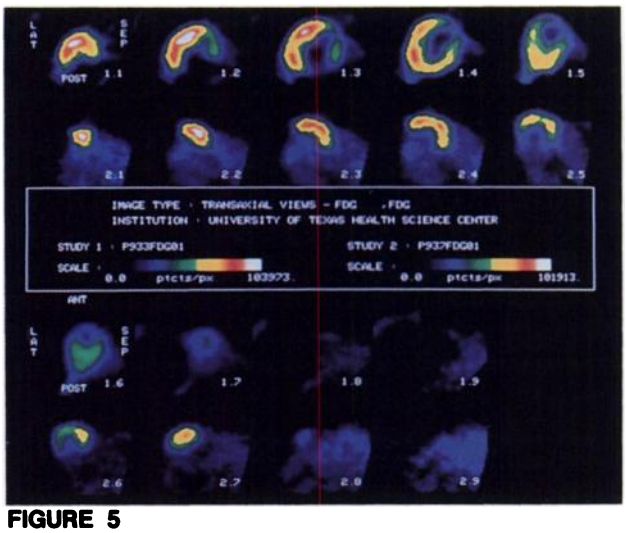

FIGURE 5
FDG tomographs obtained after glucose loading (S1 or upper row of each paired rows of images) and after fasting (S2 or lower row of each paired rows of images). Orientation of images and color scaling are as described for Figure 3A.

loading, even after their usual dose of insulin and/or oral hypoglycemic agents. Therefore, diabetic myocardium behaves as in a fasting patient, where normal FDG uptake is suppressed within the 45–90-min period of imaging when non-diabetics take up FDG. In addition, in the *fasting state at rest* in normal and diabetic subjects, FDG uptake either with or without evolving myocardial infarction is so variable as to be uninterpretable. Finally, after *fasting at rest in the setting of acute evolving MI*, intense FDG uptake may occur in areas of myocardium that are necrotic documented by lack of FDG uptake after glucose loading, left ventricular akinesis, and arteriographic involvement of the corresponding coronary artery. For these patients, necrotic tissue may appear viable due to intense FDG uptake. Similar FDG uptake in necrotic myocardium has been observed in experimental animals (*66*). In our early experience before recognizing these problems, two such patients had bypass surgery on the basis of intense FDG uptake in the occluded artery distribution after fasting but demonstrated no recovery of function and remained in chronic heart failure postoperatively despite open bypass grafts.

The mechanism for FDG uptake in recently infarcted myocardium is unclear. In experimental chronic cerebral infarction, elevated FDG uptake is observed in infarcted tissue in association with white blood cell phagocytosis of cellular debris (*67*). FDG uptake by white blood cells in MI in acute short-term experiments (6 hr) is insufficient (*68*) to explain these observations. However, longer term experiments on white blood cell uptake of FDG in evolving MI comparable to those observed for cerebral infarction or comparable to our observations in man have not been performed. Consequently, FDG uptake in evolving MI after fasting which we observed may be associated with phagocytic activity of white blood cells as found in cerebral infarction (*67*).

Stress-Perfusion Imaging for Assessing Myocardial Necrosis and Viability in Man

Several reports have defined myocardial viability in terms of stress-perfusion defects that reverse with redistribution after thallium stress testing (*69–74*) or by separate rest-stress imaging with nitrogen-13-ammonia by PET (*1*). Metabolic imaging by PET has been compared to thallium-201 for assessing viability (*11,75–77*). However, it is not appropriate to compare reversible stress-perfusion defects with resting metabolic abnormalities since they provide different information. Stress-perfusion defects not present at rest or redistribution indicate areas of limited coronary flow reserve that are measures of zones at risk, not viability per se. For severe stenoses that reduce resting flow, the defect severity on stress-perfusion images may be more intense and/or larger than at rest simply because adjacent areas with normal flow reserve have greater perfusion tracer activity associated with higher stress flow unrelated to viability in the perfusion defect. Thus, reversible stress defects reflect flow capacity of normal myocardium around a resting defect but do not provide information on viability of myocardium within a resting perfusion defect.

With reperfusion, the definition of viability as metabolically active (or not) tissue with low flow becomes unusable since the artery is patent with adequate flow and the zone at risk contains a mix of viable and necrotic tissue. In this case, stress-induced enlargement of a perfusion defect may indicate additional zones at risk with low coronary flow reserve around the damaged area or limited flow capacity in the central defect due to edema or obliteration of vascular channels. However, it does not provide information on whether there is viable myocardium in the more central reperfused area of injury.

Based on its feasibility shown here, assessing cell membrane integrity with the potassium analogue, ^{82}Rb, appears useful for clinically evaluating myocardial viability and infarct size. Since our results were obtained using a cesium-fluoride PET scanner with coincidence windows of 6 msec, further studies may be necessary to achieve these results with standard BGO detectors.

ACKNOWLEDGMENTS

The authors thank Keri Hicks, Mary Knoll Cheng, Mark Franceschini for technical assistance and David Sease, David Cassidy, and Adjit Adyanthaya for clinical support.

The authors are indebted to Claire Finn and Kathryn Rainbird for organizational support and manuscript preparation and to Ro Edens whose talented administrative management made this work possible.

Supported in part by NIH grants R01-HL26862, HL-26885, HL-28356 and as a joint collaborative project with the Clayton Foundation for Research.

REFERENCES

1. Tamaki N, Yonekura Y, Yamashita K, et al. Value of rest-stress myocardial positron tomography using nitrogen-13-ammonia for the preoperative prediction of reversible asynergy. *J Nucl Med* 1989;30:1302–1310.
2. Schelbert HR, Buxton D. Insights into coronary artery disease gained from metabolic imaging. *Circulation* 1988;78:496–505.
3. Tillisch J, Brunken R, Marshall R, et al. Reversibility of cardiac wall-motion abnormalities predicted by positron tomography. *N Engl J Med* 1986;314:884–888.
4. Brunken R, Tillisch J, Schwaiger M, et al. Regional perfusion, glucose metabolism, and wall motion in patients with chronic electrocardiographic Q-wave infarctions: evidence for persistence of viable tissue in some infarct regions by positron emission tomography. *Circulation* 1986;73:951–963.
5. Camici P, Ferrannini E, Opie LH. Myocardial metabolism in ischemic heart disease: basic principles and application to imaging by positron emission tomography. *Prog Cardiovasc Dis* 1989;32:217–238.
6. Geltman EM, Biello D, Welch MJ, Ter-Pogossian MM, Roberts R, Sobel BE. Characterization of transmural myocardial infarction by positron-emission tomography. *Circulation*

1982;65:747–755.
7. Grover-McKay M, Schelbert HR, Schwaiger M, et al. Identification of impaired metabolic reserve by atrial pacing in patients with significant coronary artery stenosis. *Circulation* 1986;74:281–292.
8. Camici P, Araujo LI, Spinks T, et al. Increased uptake of ^{18}F-fluorodeoxyglucose in postischemic myocardium of patients with exercise-induced angina. *Circulation* 1986;74:81–88.
9. Schwaiger M, Brunken R, Grover-McKay M, et al. Regional myocardial metabolism in patients with acute myocardial infarction assessed by positron emission tomography. *J Am Coll Cardiol* 1986;8:800–808.
10. Marshal RC, Tillisch JH, Phelps ME, et al. Identification and differentiation of resting myocardial ischemia and infarction in man with positron computed tomography, ^{18}F-labeled fluorodeoxyglucose, and N-13-ammonia. *Circulation* 1983; 67:766–778.
11. Brunken K, Schwaiger M, Grover-McKay M, Phelps M, Tillisch J, Schelbert H. Positron emission tomography detects tissue metabolic activity in myocardial segments with persistent thallium perfusion defects. *J Am Coll Cardiol* 1987;10:557–567.
12. de Jong JW, Goldstein S. Changes in coronary venous inosine concentration and myocardial wall thickening during regional ischemia in the pig. *Circ Res* 1974;35:111–116.
13. de Jong JW, Verdouw PD, Remme WJ. Myocardial nucleoside and carbohydrate metabolism and hemodynamics during partial occlusion and reperfusion of pig coronary artery. *J Mole Cell Cardiol* 1977;9:297–312.
14. Owen P, Thomas M, Young V, Opie L. Comparison between metabolic changes in local venous and coronary sinus blood after acute experimental coronary arterial occlusion. *Am J Cardiol* 1970;25:562–570.
15. Opie LH, Thomas M, Owen P, Shulman G. Increased coronary venous inorganic phosphate concentrations during experimental myocardial ischemia. *Am J Cardiol* 1972;30:503–513.
16. Case RB, Nasser MG, Crampton RS. Biochemical aspects of early myocardial ischemia. *Am J Cardiol* 1969;24:766–775.
17. Hill JL, Gettes LS. Effect of acute coronary artery occlusion on local myocardial extracellular K+ activity in swine. *Circulation* 1980;61:768–777.
18. Shine KI. Ionic events in ischemia and anoxia. *Am J Pathol* 1981;102:256–261.
19. Nakaya H, Kimura S, Kanno M. Intracellular K+ and Na+ activities under hypoxia, acidosis, and no glucose in dog hearts. *Am J Physiol* 1985;249:H1078–1085.
20. Conrad GL, Rau EE, Shine KI. Creatine kinase release, potassium-42 content and mechanical performance in anoxic rabbit myocardium. *J Clin Invest* 1979;64:155–161.
21. Johnson RN, Sammel NL, Norris RM. Depletion of myocardial creatine kinase, lactate dehydrogenase, myoglobin, and K+ after coronary artery ligation in dogs. *Cardiovasc Res* 1981;15:529–537.
22. Tancredi RG, Yipintsoi T, Bassingthwaighte JB. Capillary and cell wall permeability to potassium in isolated dog hearts. *Am J Physiol* 1975;229:537–544.
23. Poe ND. Comparative myocardial uptake and clearance characteristics of potassium and cesium. *J Nucl Med* 1972;7:557–560.
24. Ishii Y, MacIntyre WJ, Pritchard WH. Measurement of total myocardial blood flow in dogs with ^{43}K and the scintillation camera. *Circ Res* 1973;33:113–122.
25. Prokop EK, Strauss HW, Shaw J, Pitt B, Wagner HN. Comparison of regional myocardial perfusion determined by ionic potassium-43 to that determined by microspheres. *Circulation* 1974;50:978–984.
26. Zaret BL, Strauss HW, Martin ND, Wells HP, Flamm MD. Noninvasive regional myocardial perfusion with radioactive potassium. Study of patients at rest, with exercise, and during angina pectoris. *N Engl J Med* 1973;288:809–812.
27. Ziegler WH, Goresky CA. Kinetics of rubidium uptake in the working dog heart. *Circ Res* 1971;29:208–220.
28. Sheehan RM, Renkin EM. Capillary, interstitial, and cell membrane barriers to blood-tissue transport of potassium and rubidium in mammalian skeletal muscle. *Circ Res* 1972;30:588–607.
29. Yipintsoi T, Dobbs WA, Scanlon PD, Knopp TJ, Bassingthwaighte JB. Regional distribution of diffusible tracers and carbonized microspheres in the left ventricle of isolated dog hearts. *Circ Res* 1973;33:573–587.
30. Holman BL, Eldh P, Adams DF, Han MH, Poggenburg JK, Adelstein SJ. Evaluation of myocardial perfusion after intracoronary injection of radiopotassium. *J Nucl Med* 1973;14:274–278.
31. Schelbert HR, Ashburn WL, Chauncey DM, Halpern SE. Comparative myocardial uptake of intravenously administered radionuclides. *J Nucl Med* 1974;15:1092–1100.
32. Nishiyama H, Sodd VJ, Adolph RJ, Saenger EL, Lewis HT, Gabel M. Intercomparison of myocardial imaging agents: ^{201}Tl, ^{129}Cs, ^{43}K, and ^{81}Rb. *J Nucl Med* 1976;17:880–889.
33. Selwyn AP, Allan RM, L'Abbate A, et al. Relation between regional myocardial uptake of rubidium-82 and perfusion: absolute reduction of cation uptake in ischemia. *Am J Cardiol* 1982;50:112–121.
34. Love WD, Ishihara Y, Lyon LD, Smith RO. Differences in the relationships between coronary blood flow and myocardial clearance of isotopes of potassium, rubidium, and cesium. *Am Heart J* 1968;76:353–355.
35. Love WD. Isotope clearance and myocardial blood flow. *Am Heart J* 1964;67:579–582.
36. Bing RJ, Bennish A, Bluemchen G, Cohen A, Gallagher HP, Zaleski EJ. The determination of coronary flow equivalent with coincidence counting technique. *Circulation* 1964; 29:833–846.
37. Moir TW. Measurement of coronary blood flow in dogs with normal and abnormal myocardial oxygenation and function. *Circ Res* 1966;14:695–699.
38. McHenry PL, Knoebel SB. Measurement of coronary blood flow by coincidence counting and a bolus of $^{84}RbCl_1$. *J Appl Physiol* 1967;22:495–500.
39. Mymin D, Sharma GP. Total and effective coronary blood flow in coronary and noncoronary heart disease. *J Clin Invest* 1974;53:363–373.
40. Becker L, Ferreira R, Thomas M. Comparison of ^{86}Rb and microsphere estimates of left ventricular blood flow distribution. *J Nucl Med* 1974;15:969–973.
41. Knoebel SB, Lowe DK, Lovelace DE, Friedman KI. Myocardial blood flow as measured by fractional uptake of rubidium-84 and microspheres. *J Nucl Med* 1978;19:1020–1026.
42. Downey HF, Bashour FA, Parker PE, Bashour CA, Rutherford CS. Myocardial and total-body extractions of radiorubidium in anesthetized dogs. *J Appl Physiol* 1975;38:31–32.
43. Cohen MV. Quantitation of collateral and ischemic flows with microspheres and diffusible indicator. *Am J Physiol* 1978;234:487–495.
44. Mullani NA, Gould KL. First-pass regional blood flow measurements with external detectors. *J Nucl Med* 1983;24:577–581.
45. Mullani NA, Goldstein RA, Gould KL, Fisher DJ, Marani SK, O'Brien HA. Myocardial perfusion with rubidium-82. I. Measurement of extraction fraction and flow with external detectors. *J Nucl Med* 1983;24:898–906.
46. Goldstein RA, Mullani NA, Fisher D, Marani S, Gould KL, O'Brien HA. Myocardial perfusion with rubidium-82. II. The effects of metabolic and pharmacologic interventions. *J Nucl*

Med 1983;24:907–915.
47. Cohen A, Zaleski EJ, Luebs ED, Bing RJ. The use of positron emitter in the determination of coronary blood flow in man. *J Nucl Med* 1965;6:651–666.
48. Cohen A, Gallagher JP, Luebs ED, et al. The quantitative determination of coronary flow with a positron emitter (rubidium-84). *Circulation* 1965;32:636–649.
49. Donato L, Bartolomei G, Federighi G, Torreggiani G. Measurement of coronary blood flow by external counting with radioactive rubidium. *Circulation* 1966;33:708–718.
50. Cohen A, Zaleski EJ, Baleiron H, Stock TB, Chiba C, Bing RJ. Measurement of coronary blood flow using rubidium-84 and the coincidence counting method. *Am J Cardiol* 1967;19:556–562.
51. Cowan C, Duran PVM, Corsini G, Goldschlager N, Bing RJ. The effects of nitroglycerin on myocardial blood flow in man. *Am J Cardiol* 1969;24:154–160.
52. Knoebel SB, Elliott WC, McHenry PL, Ross E. Myocardial blood flow in coronary artery disease. Correlation with severity of disease and treadmill exercise response. *Am J Cardiol* 1971;27:51–58.
53. Lurie AJ, Salel AF, Berman DS, DeNardo GL, Hurley EJ, Mason DT. Determination of improved myocardial perfusion after aortocoronary bypass surgery by exercise rubidium-81 scintigraphy. *Circulation* 1976;54(suppl 3):III-20–23.
54. Goldstein RA, Mullani NA, Wong WH, et al. Positron imaging of myocardial infarction with rubidium-82. *J Nucl Med* 1986;27:1824–1829.
55. Yano Y, Cahoon JL, Budinger TF. A precision flow-controlled Rb-82 generator for bolus or constant-infusion studies of the heart and brain. *J Nucl Med* 1981;22:1006–1010.
56. Neirinckx RD, Kronauge JF, Gennaro GP. Evaluation of inorganic absorbents for rubidium-82 generator. I. Hydrous Sno_2. *J Nucl Med* 1982;24:898–906.
57. Gould KL, Goldstein RA, Mullani NA, et al. Non-invasive assessment of coronary stenoses by myocardial perfusion imaging during pharmacologic coronary vasodilation. VIII. Clinical feasibility of positron cardiac imaging without a cyclotron using generator-produced rubidium-82. *J Am Coll Cardiol* 1986;7:775–789.
58. Demer LL, Gould KL, Goldstein RA, et al. Assessment of coronary artery disease severity by positron emission tomography. Comparison with quantitative arteriography in 193 patients. *Circulation* 1989;79:825–835.
59. Goldstein RA. Kinetics of rubidium-82 after coronary occlusion and reperfusion. *J Clin Invest* 1985;75:1131–1137.
60. Hicks K, Ganti G, Mullani N, Gould KL. Automated quantitation of 3-D cardiac PET for routine clinical use. *J Nucl Med* 1989;30:1787–1797.
61. Mullani N, Wong W, Hartz R, Philippe E, Yerian K. Sensitivity improvement of TOFPET by the utilization of the interslice coincidence. *IEEE Trans Nucl Sci* 1982;NS-29, No. 1:479–483.
62. Mullani NA, Gaeta J, Yerian K, et al. Dynamic imaging with high resolution time-of-flight PET camera—TOFPET I. *IEEE Trans Nucl Sci* 1984;NS-31, No. 1:609–613.
63. Wong WH, Mullani NA, Phillipe EA, Hartz R, Gould KL. Image improvement and design optimization of the time-of-flight PET. *J Nucl Med* 1983;24:52–60.
64. Mullani NA, Gould KL, Hartz RK, et al. Design and performance of Posicam 6.5 BGO Positron Camera. *J Nucl Med* 1990;31:610–616.
65. Snedecor GW, Cochran WG. *Statistical methods*, 6th edition. Ames, Iowa: Iowa State University Press; 1976.
66. Bianco JA, Bakanauskas J, Carlson M, et al. Augmented uptake of 2-C-14-D-deoxyglucose in reversibly-injured myocardium. *Eur J Nucl Med* 1988;13;557–562.
67. Komatsumoto S, Greenberg JH, Hickey WF, Reivich M. Local cerebral glucose utilization in chronic middle cerebral artery occlusion in the cat. *J Cereb Blood Flow Metab* 1989;9:535–547.
68. Wijns W, Jacque AM, Leners N, et al. Accumulation of polymorphonuclear leukocytes in reperfused ischemic canine myocardium: relation with tissue viability assessed by fluorine-18-2-deoxyglucose uptake. *J Nucl Med* 1988;29:1826–1832.
69. Bodenheimer MM, Banka VS, Fooshee C, Hermann GA, Helfant RH. Relationship between regional myocardial perfusion and the presence, severity and reversibility of asynergy in patients with coronary heart disease. *Circulation* 1978;58:789–878.
70. Rozanski A, Berman DS, Gray R, et al. Use of thallium-201 redistribution scintigraphy in the preoperative differentiation of reversible and nonreversible myocardial asynergy. *Circulation* 1981;64:936–944.
71. Iskandrian AS, Hakki A-H, Kane SA, Goel IP, Mudth ED, Segal BL. Rest and redistribution thallium-201 myocardial scintigraphy to predict improvement in left ventricular function after coronary arterial bypass grafting. *Am J Cardiol* 1983;51:1312–1316.
72. Cloninger KG, DePuey EG, Garcia EV, et al. Incomplete redistribution in delayed thallium-201 single photon emission computed tomographic (SPECT) images: an overestimation of myocardial scarring. *J Am Coll Cardiol* 1988;12:955–963.
73. Galli M, Bencivelli W, Pardo NF, Tavazzi L. Underestimation of residual ischemia by thallium-201 scintigraphy after myocardial infarction. *Chest* 1988;94:876–878.
74. Tamaki N, Yonekura Y, Yamashita K, et al. Relation of left ventricular perfusion and wall motion with metabolic activity in persistent defects on ^{201}Tl tomography in healed myocardial infarction. *Am J Cardiol* 1988;62:202–208.
75. Tamaki N, Yonekura Y, Senda M, et al. Value and limitation of stress ^{201}Tl single-photon emission computed tomography: comparison with ^{13}N-ammonia positron tomography. *J Nucl Med* 1988;29:1181–1188.
76. Brunken RC, Kottou S, Nienaber CA, et al. PET detection of viable tissue in myocardial segments with persistent defects at Tl-201 SPECT. *Radiology* 1989;172:65–73.
77. Melin JA, Wijns W, Keyeux A, et al. Assessment of thallium-201 redistribution versus glucose uptake as predictors of viability after coronary occlusion and reperfusion. *Circulation* 1988;77:927–934.